Strength Analysis of Structurally Optimized Aluminium-Composite Tubular Lap Joints

M. Jäger ✉ and S. Wartzack

Friedrich-Alexander-Universität Erlangen-Nürnberg, Germany

✉ jaeger@mfk.fau.de

Abstract

Truss structures are a stiff, economical, and efficient lightweight design, the limiting factor of these structures are usually the load transfer elements. This paper presents an analytical design method for optimized adhesive tubular lap joints between CFRP tubes and aluminium inserts. The analytically optimized design agrees very well with the numerical simulations and experimental results. Although the experiments show a highly non-linear behaviour, where a linear elastic correlation is expected, the total load capacity is only reached when the adhesive is fully plasticised.

Keywords: lightweight design, design optimisation, tubular lap joint, experimentation, composites

1. Introduction

Spatial truss structures are a stiff, economical, and efficient lightweight design (Pasternak *et al.*, 2010; Klein, 2017), especially if composites like carbon fibre reinforced polymers (CFRP) are used for the struts. In combination with standardised profile geometry and fixed sizes, competitive prices can be achieved compared to classical materials used for truss structures. However, the limiting factor of these structures are usually the load transfer elements between the CFRP struts (Schütze, 1997) which need to be optimised in order to realise their full lightweight potential. Due to the multiaxial stress state in the connection points (nodes), these nodes are commonly made from isotropic lightweight materials like aluminium or titanium. However, initial solutions made of CFRP already exist (CG TEC GmbH, 2021). Various methods can be used to join CFRP and aluminium. An overview is given by Pramanik *et al.* (2017), containing adhesive bonding, self-piercing rivets, diffusion bonding, bolted joints, clinching and welding. Furthermore, the form locking joint (Figure 1b) presented by Schütze (1997) is a very effective way for transmitting high axial loads, but the individualized struts are expensive to manufacture due to the need of customizing every single one.
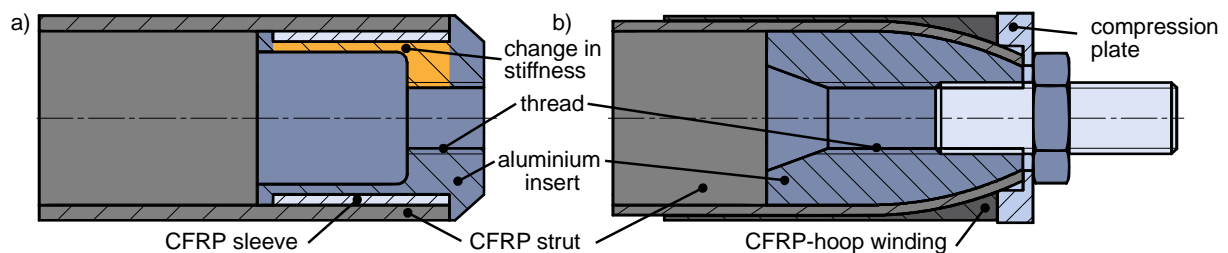

Figure 1. Joints by Schütze; a) adhesive joint; b) form locking joint (Walbrun *et al.*, 2019)

On the other hand, the presented adhesive joint by Schütze (Figure 1a) is a simple and easy to manufacture concept, compatible with standardised profile geometry and fixed sizes of struts. Therefore, this type of connection is suitable for an effective and economical lightweight truss structure and is considered and optimized in the following. The goal of this paper is to provide a design method for optimized adhesive tubular lap joints to connect standardized CFRP tubes with fixed diameters to aluminium inserts for static load cases. The analytical stress distribution of the optimized designs is then compared to numerical simulations and experimental tests.

2. Optimized Design

The stress distribution along lap joints, especially between different materials, is highly non-linear. To design an optimal joint, it must be considered during the design process. A lot of different mechanical models exist, for example a model for cylindrical adhesive joints by Nemeş et al. (2006), a model with a hyperbolic stress distribution by Volkersen (1938), a model by Hart-Smith (1973) including partial plasticity at the ends of the lap joint and many others. In case of a structural lap joint, only elastic deformation of the adhesive is permissible, therefore the model by Hart-Smith is omitted. The model by Nemeş et al. assumes the shear stresses at the ends of the lap joint vanish, differing from the stress distributions presented by Adams and Peppiatt (1977), Lubkin and Reissner (1956), Schürmann (2007) and Habenicht (2009). The model predicts a parabolic stress distribution for short joining lengths with the maximum located in the middle of the joint (Nemeş et al., 2006). For lightweight design reasons, the overlap length should be kept as short as possible, while the stress distribution model must remain valid for short lengths. Due to these considerations, the model presented by Nemeş et al. is not used either. The hyperbolic stress distribution model by Volkersen has none of these limitations but was developed for single lap joints and needs to be modified to be applicable to tubular joints.

2.1. Modified Volkersen model

The geometrical and material definitions of the joint are shown in Figure 2. Both the outer CFRP tube and the inner aluminium insert are assumed prismatic, the Young's modulus is denoted by E, the shear modulus by G.
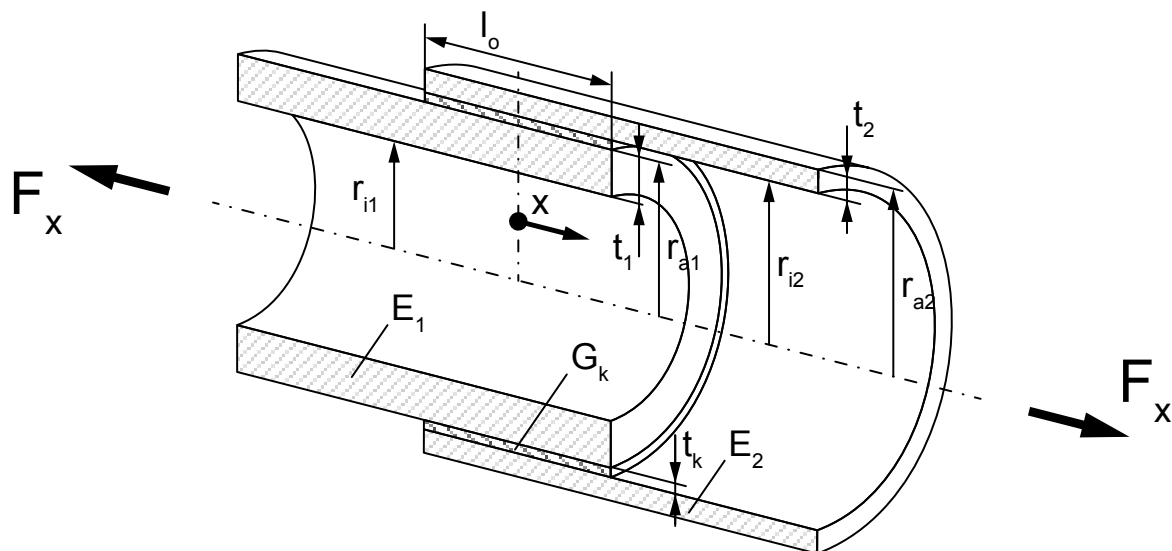

Figure 2. Geometrical and material definitions of the tubular lap joint

To modify the model by Volkersen, the width b of the lap joint is replaced by the perimeter w along the midline of the adhesive layer. The sheet thickness t_i therefore is replaced by $\frac{A_i}{w}$. This results in the modified differential Equation 1 with $n_{xy}(x) = w\,\tau_K(x)$ denoting the shear flow within the adhesive.

$$\left[\frac{1}{E_1\frac{A_1}{w}} + \frac{1}{E_2\frac{A_2}{w}}\right] n_{xy}(x) - \frac{t_K}{G_K}\, n_{xy}''(x) = 0 \qquad (1)$$

ENGINEERING DESIGN PRACTICE

The resulting shear stress distribution is shown in Equation 2, with ψ being the stiffness ration of the tubes and ρ denoting a characteristic adhesion ratio depending on the dimensional and mechanical specifications of the tubes and the adhesive (Schürmann, 2007). The shear stress distribution function is abbreviated by $S_\mathrm{p}(x)$ and is scaling the average shear stress $\overline{\tau}_K = \frac{F_x}{w\, l_0}$ of the joint.

$$\tau_K(\mathrm{x}) = \frac{\rho}{2}\left[\frac{\cosh(\rho x/l_o)}{\sinh(\rho/2)} - \frac{(1-\Psi)\,\sinh(\rho x/l_o)}{(1+\Psi)\,\cosh(\rho/2)}\right]\overline{\tau}_K = S_p(x)\,\overline{\tau}_K \tag{2}$$

The stiffness ratio ψ and the characteristic adhesion ratio ρ are provided in Equations 3 and 4.

$$\Psi = \frac{E_1 A_1}{E_2 A_2} \tag{3}$$

$$\rho = l_o \sqrt{\frac{(1+\Psi)G_K}{E_1 \frac{A_1}{w} t_K}} \tag{4}$$

2.2. Parameter variations

As can be seen from Equations 2 to 4, the shear stress distribution along the lap joint is highly non-linear and depends strongly on various geometric and material factors. In order to achieve an optimal design, these factors are analysed and optimized in the following section.

Stiffness ratio

The first factor to consider is the stiffness ratio ψ (Equation 3), a stiffness ratio less than 1 implies the outer tube made from CFRP is stiffer than the aluminium insert and vice versa. The stress distribution function $S_\mathrm{p}(x)$ for a joint of a length of 20 mm is illustrated in Figure 3. An equal stiffness of both joint partners results in a symmetric stress distribution with the overall lowest stress peaks at the ends of the joint. By deriving from the stiffness ratio of 1, the stress peak at one end decreases, while the peak at the other end increases. An optimal designed tube joint thus consists of equal stiffnesses ($E_1 A_1 = E_2 A_2$).
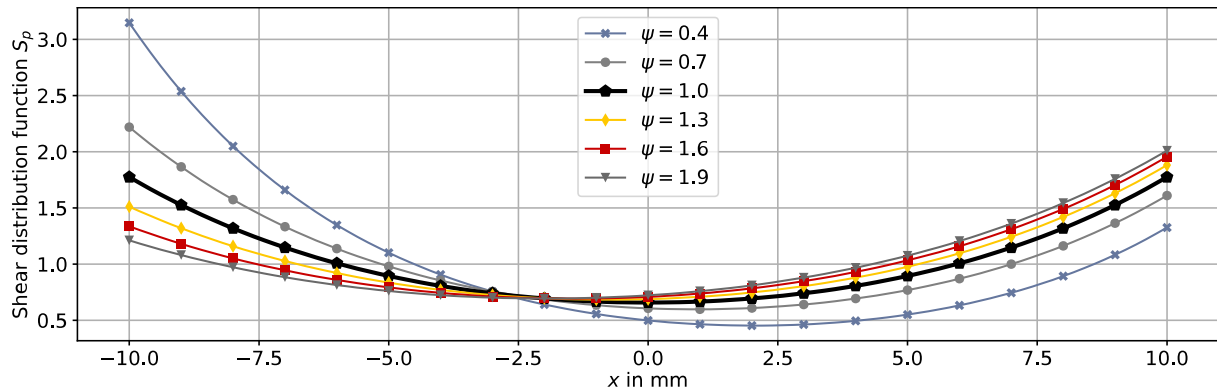

Figure 3. Shear stress distribution along the lap joint for varying stiffness ratios ψ

Lap joint length

The next factor to consider is the joint length l_o, which affects the characteristic adhesion ratio ρ (Equation 4). An increasing length of the joint is therefore accompanied with a decreasing average shear stress $\overline{\tau}_K$, which results in decreasing peak stresses. But considering Equation 2, the peak stresses at the ends of the joint are no longer decreasing for a characteristic adhesion ratio $\rho = 5$ and above. The corresponding joint length for $\rho = 5$ is called critical overlap length $l_{o,\mathrm{crit}}$, above which the strength of the joint does not increase further (Schürmann, 2007). The critical length is shown below in Equation 5 and depends on the geometrical and material properties of the joint.

$$l_{o,krit} = 5\sqrt{\frac{\Psi E_1 A_1 t_K}{G_K(1+\Psi)w}} \overset{\psi=1}{=} 5\sqrt{\frac{E_1 A_1 t_K}{2 G_K w}} \tag{5}$$

ENGINEERING DESIGN PRACTICE

A plot for varying lap joint lengths in relation to the critical length is shown in Figure 4. From a lightweight design perspective, the optimal joint length is thus given by the critical length $l_{o,crit}$. Following the manufacturing guidelines presented by Siebert (2006), the overlap length is determined by the average adhesive diameter of the joint ($0 \leq l_0 \leq 2\,D_m$). The critical length presented fits well within this guideline. However, the ultimate strength of the joint depends almost entirely on the stiffness of the material and remains nearly constant for changes in diameter. By only following geometrical guidelines, the joint length can easily be oversized, and the full lightweight potential thus not utilised.
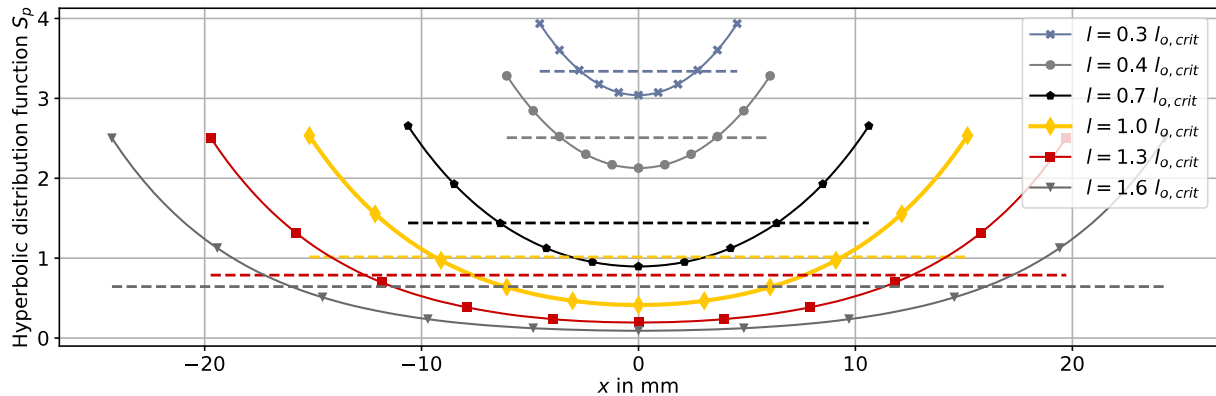

Figure 4. Shear stress distribution along the lap joint for varying lap joint lengths

Additional design requirements

In addition to the geometric optimization of the joint, process-related criteria should also be taken into account. To further increase the strength of the joint, the adhesive will be applied by injection bonding. Measurements by Siebert (2006) and Albiez (2016) proved, that injecting the adhesive into the joint gap significantly increases the strength compared to manual application and wet assembly. Therefore, the design must also consider the geometric requirements for injection bonding, shown in Figure 5. Such as minimum gap size, injection ports/vent holes and alignment features.
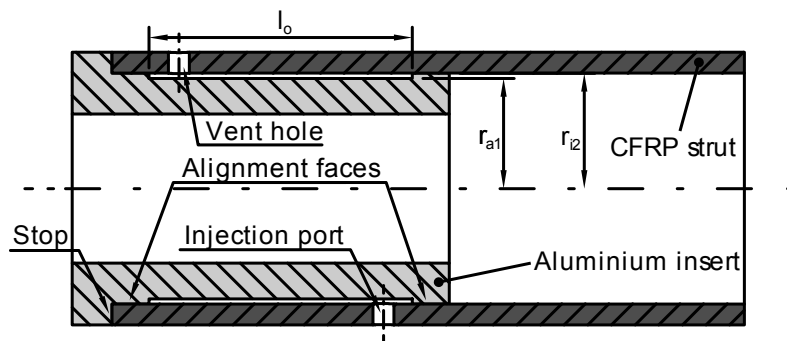

Figure 5. Geometric requirements for injection bonding

Resulting design

The optimized design which meets all the requirements above is shown in Figure 6. While the design is somewhat similar to the ones presented by Siebert (2006) and Schütze (1997), it differs in various points. Unlike the design by Schütze, the threaded portion of the insert does not overlap with the adhesive joint, thus inducing no stiffness change, compare Figure 6 - A to Figure 1a - yellow marking. As shown in Figure 3, a stiffer aluminium insert compared to the outer tube ($\Psi > 1$) results in an increased stress peak at the end of the joint, which decreases the strength of the joint significantly. Due to the manufacturing process of the CFRP tubes (winding), the tolerances of their inner diameter can be kept very small. Therefore the use of gaskets between the tubes (Siebert, 2006) is not strictly necessary for sealing and is avoided for cost and lightweight reasons. The sealing is realised by a very

small gap between the concentric surfaces marked in Figure 6 at position B. As adhesive, Scotch-Weld™ DP 490 with a shear modulus of $G_K = 1500$ N/mm^2 is used, the adhesive thickness is chosen as $t_k = 0.5$ mm due to manufacturing restrictions of the injection bonding process and the viscosity of the adhesive. Chamfers (15°) are added for easier assembly (Figure 6 - C). To minimise the post-processing of the CFRP tube when cut to length, an undercut is incorporated at position D in Figure 6.
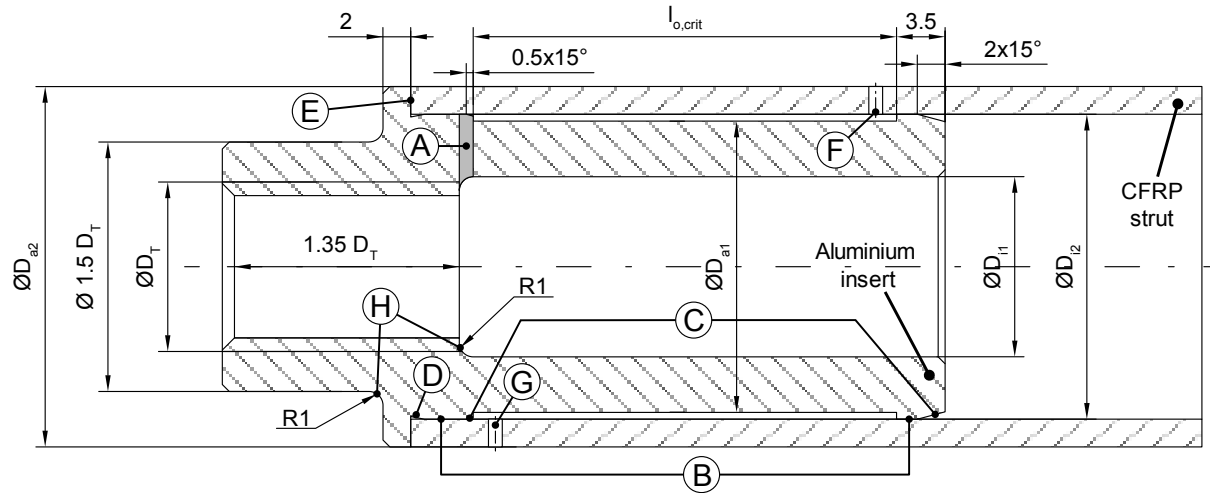
Figure 6. Optimized design

To avoid assembly jigs, a stop is provided at point E. Due to the small size of the tubes, only one injection port (Figure 6 - F) and vent hole (Figure 6 - G) is included in this design. To facilitate injection bonding for larger diameters, an increased number of injections ports and vent holes should be considered. Radii at remarks H in Figure 6 avoid stress concentration at the diameter changes of the insert. For demonstration purposes, three different CFRP laminates with a total thickness of 2 mm are used, their composition and mechanical properties are shown in Table 1.

Table 1. Laminate composition and mechanical properties along the longitudinal axis x and along the perimeter s

Ply angle	Layer thickness [mm]	E_x [MPa]	E_s [MPa]	G_{xs} [MPa]	v_{xs}	v_{sx}
[90°, 12°, -12°]$_2$	[0.2, 0.4, 0.4]$_2$	100 600	34 900	8 600	0,065	0,188
[90°, 25°, -25°]$_2$	[0.2, 0.4, 0.4]$_2$	70 600	35 000	18 850	0,217	0,438
[90°, 35°, -35°]$_2$	[0.2, 0.4, 0.4]$_2$	43 200	36 100	26 100	0,433	0,519

Each of the three laminates will be combined with three different standardized strut diameters (18 mm, 22 mm, 26 mm) to create a total number of nine different inserts. The resulting design parameters matching Figure 6 are listed in Table 2. It is noticeable - the overlap length depends almost exclusively on the laminate properties and not on the geometric dimensions (diameter).

Table 2. Resulting insert designs for three different laminates and CRFP tube diameters

D_{i2} [mm]	D_{a2} [mm]	E_x [MPa]	$l_{o,crit}$ [mm]	D_{i1} [mm]	D_{a1} [mm]	D_T [mm]
18	**22**	**100 600**	**30.9**	**7.8**	**17**	**M10**
18	22	70 600	25.8	11.4	17	M10
18	22	43 200	19.5	14.0	17	M10
22	**26**	**100 600**	**30.5**	**13.0**	**21**	**M12**
22	26	70 600	25.5	15.8	21	M12
22	26	43 200	19.3	18.2	21	M12
26	**30**	**100 600**	**30.2**	**17.4**	**25**	**M12**
26	30	70 600	25.3	20.0	25	M12
26	30	43 200	19.1	22.2	25	M12

3. Numerical Comparison

In this section, the optimized design is compared to a model in Ansys 2021R1 using the Ansys Composite PrepPost module (ANSYS, 2021) to model the CFRP laminate ply-wise with solid elements within the finite element analysis, the discretization of the model is shown in Figure 7. Bias meshing is introduced at the ends of the adhesive layer to further refine the results.
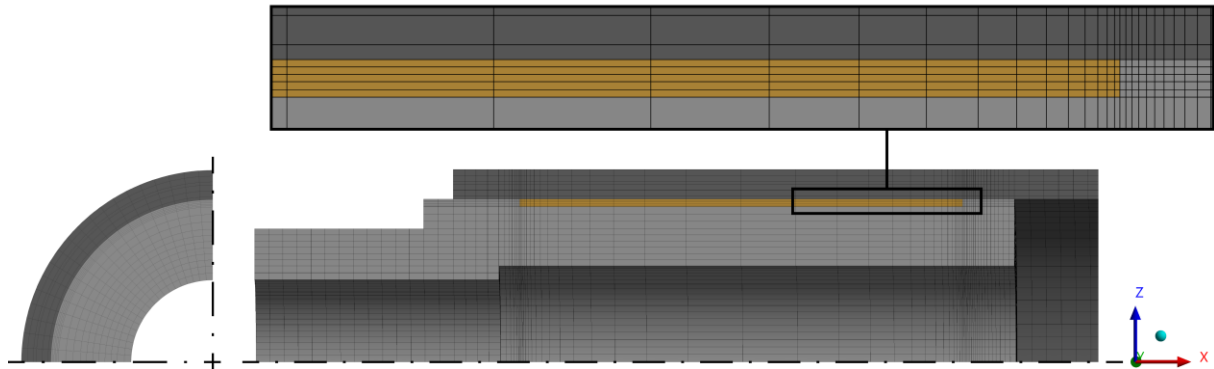

Figure 7. Finite element model for comparison to the analytical stress distribution

Shear stress

The resulting shear stress distribution is exemplarily shown in Figure 8 for the insert with D_{i2} = 22 mm, E_2 = 100 600 N/mm^2 and an axial force of F_x = 21 kN. The shear stress is evaluated on the inside, the middle and the outside faces of the adhesive layer. Except for the ends of the joint, the stresses of the numerical solution along these three paths match very well (deviation less than 3.5% for $|x| \leq$ 13.75 mm and less than 1.5% for $|x| \leq$ 12.5 mm). The stresses at $|x| > 13.75$ mm are not considered in the following due to their large deviation.
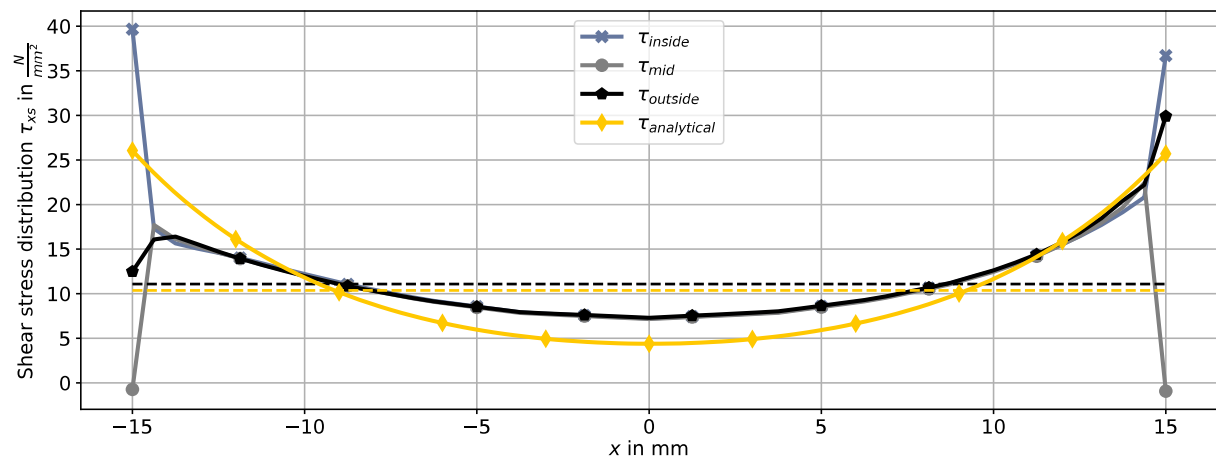

Figure 8. Comparison of the shear stress distribution for analytical and numerical solution

The shear stress distribution for the numerical solution is not completely symmetric, because of the lower stiffness of the innermost laminate layer (90° ply angle $\rightarrow \psi > 1$) compared to the overall laminate stiffness. The mean stresses (analytical: 10.4 N/mm^2, numerical: 11.1 N/mm^2) and the peak stress on the right side (x = 13.75 mm; analytical: 23.3 N/mm^2, numerical: 21.8 N/mm^2) are very similar. In the middle of the joint and at the left peak, the values differ considerably (middle: 4.39 N/mm^2 analytical vs. 7.22 N/mm^2 numerical, left: x = -13.75 mm; 23.6 N/mm^2 analytical vs. 17.0 N/mm^2 numerical) due to unequal stiffness of the layers bonded. The analytical model derived from the model by Volkersen (1938) can be therefore considered a conservative-safe estimation of the shear stress distribution, overestimating the stress peaks at the ends and underestimating the stress in the middle of the joint for a CFRP/aluminium adhesive joint.

Normal stress

Within the analytical model the normal stresses σ_{ss} (along the perimeter s) are neglected, Figure 9 shows their distribution based on the numerical solution along the length of the joint.
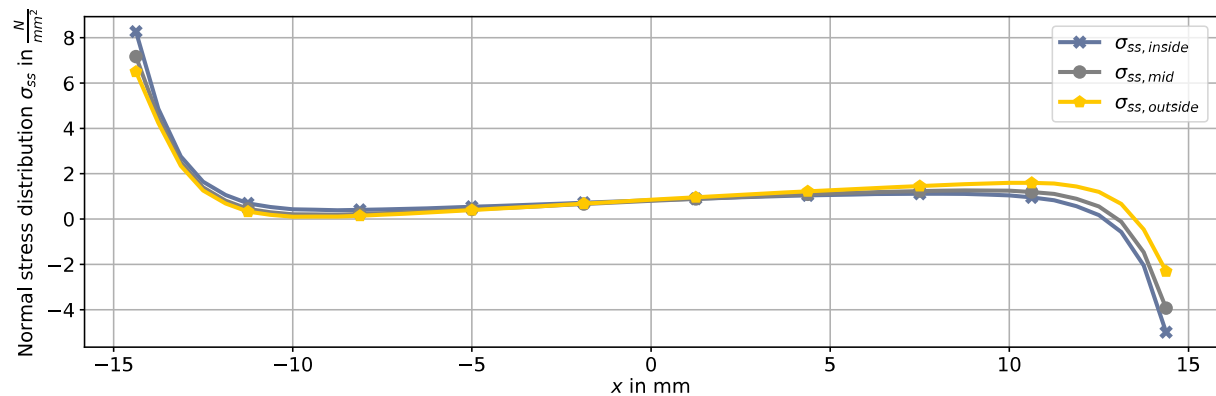

Figure 9. Normal stress distribution for the numerical solution

The qualitative progression is similar to the model presented by Nemeş *et al.* (2006), while the peaks of the stresses are much lower (by factor of 40-50) compared to his model. Due to the resulting total stresses at the end of the joint, failure at lower loads is conceivable, which will be investigated in the next section.

4. Experimental results

Tests are performed with the inserts marked in Table 2, combing each of the three inserts with each of the laminates. One combination with a stiffness ratio of $\psi = 1$ and two with stiffness ratios of $\psi > 1$ are therefore tested. The tests are performed for three different diameters of struts and five samples each. Figure 10 shows a test specimen. All specimens have a total length of 225 mm including both inserts.

Figure 10. Specimen used for tensile strength tests of the injection bonded insert

A standard tensile test rig is used, the tests are performed at a nominal speed of 1 ‰ (0,225 mm/s). The resulting load-displacement diagram for the samples with an inner diameter of 22 mm and the laminate [90°, 25°, -25°]₂ is exemplary shown in Figure 11. All other combinations of laminates and inserts showed very similar results.
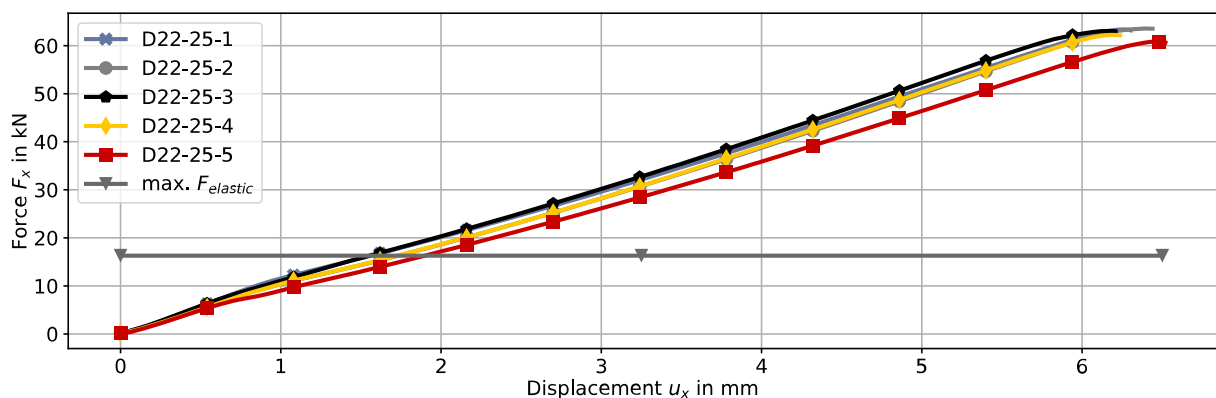

**Figure 11. Load-displacement diagram for specimens with $D_{i2} = 22\ mm$ and 25° laminate**

A change in the gradient of the load-displacement curve at a displacement $u_x \approx 0.75$ mm is recognisable and can be clearly seen in the low-pass filtered stiffness-force diagram shown in Figure 12. A highly non-linear behaviour is observed up to the expected maximum elastic force. After reaching this limit, the stiffness of the joint then increases approximately linear, presumably due to plastic deformation, until sudden total failure.
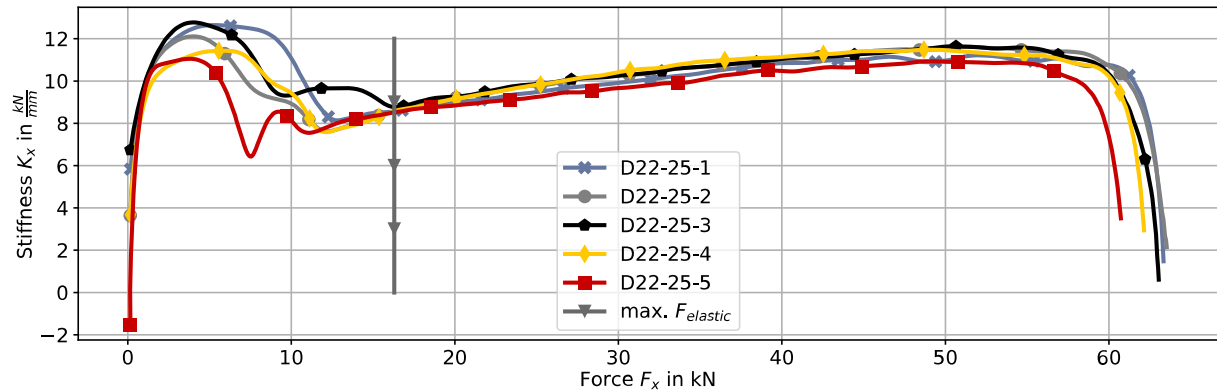
Figure 12. Stiffness-force diagram for specimens with $D_{i2} = 22\ mm$ and 25° laminate

Almost every sample failed approximately at complete plastification of the adhesive. The maximum loads reached are shown in Figure 13. They are compared to the maximum plastic load $F_{max,plastic}$ and the elastic load limit $F_{max,elastic}$ predicted by the analytical model.
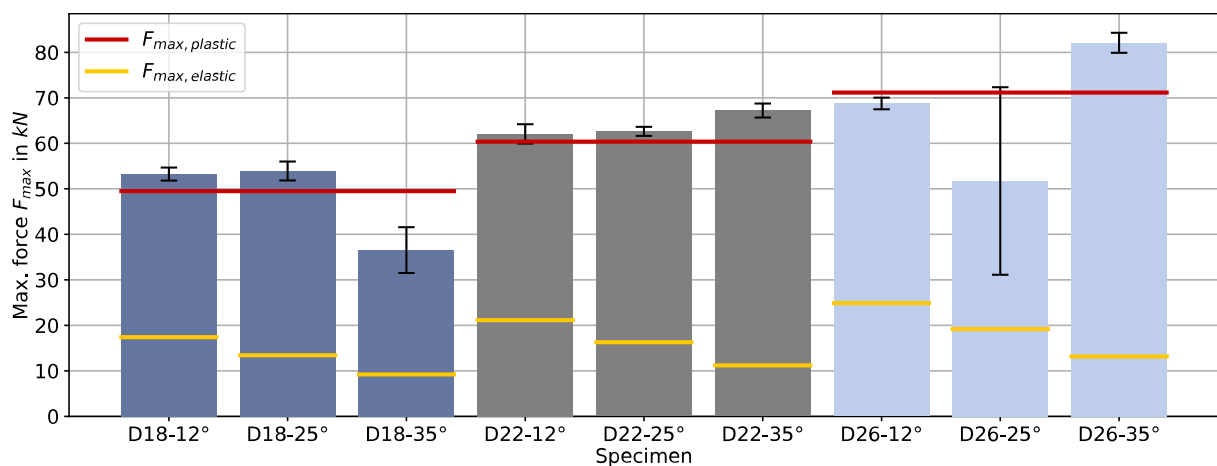
Figure 13. Maximum experimental load capacity of the joint compared to the elastic load limit and the load limit for complete plastification of the adhesive

For all five specimens D18-35° the laminate failed in the middle of the specimen instead of the adhesive of the joint (see Figure 14). In addition, two of the five specimens D26-25° were outliers and failed at a significantly lower load (less than half) compared to the other three. Therefore, the D18-35° and D26-25° results were not considered in the evaluation.

Figure 14. Failure of the laminate for specimens D18-35

Considering the different laminate types, the relation between stiffness ratio and maximum load is inverse to the one expected. The maximum sustained force increases slightly as the stiffness decreases.

          ENGINEERING DESIGN PRACTICE

Figures 15 and 16 show joints with interlaminar failure of the CFRP tube at the innermost layer, which may explain this correlation. As the difference in ply angles between the innermost layers decreases, the interlaminar load transfer capability increases and thus the maximum load capacity increases slightly.

Figure 15. Failed joint caused by interlaminar failure of the CFRP tube - sample D18-12-1

Figure 16. Failed joint caused by interlaminar failure of the CFRP tube - sample D22-35-3

5. Conclusion

A design method for an optimized tubular lab joint made from CFRP tubes and aluminium inserts based on the shear stress distribution by Volkersen has been derived. The approach not only reduced time and effort to achieve a sophisticated design, it also increases the lightweight capability compared to common design guidelines. For example, in the case of an overlap joint according to Siebert's guideline, only the geometric dimensions are taken into account, while the stiffness properties are not considered when combining different materials. According to the presented analytical model, the strength of the design model mainly depends on the stiffness ratio of the two parts. Numerical simulations of the joint have shown, that the proposed shear stress distribution adapted from Volkersen is qualitatively correct, but a conservative estimate, cf. Figure 8. Normal stresses in the circumferential direction are not taken into account in this model, which other models include (Nemeş *et al.*, 2006). Furthermore, intralaminar stiffness variations are not considered. Experimental investigations show a non-linear stiffness characteristic below the predicted maximum elastic load limit (considering only static load cases), but almost all specimens achieved complete plastification before failure regardless of the stiffness ratio of the joining parts. To further increase the lightweight potential of these connections, the author proposed to use inserts/nodes manufactured directly from short-fibre reinforced CFRP via additive manufacturing (Jäger *et al.*, 2020). However, according to the results obtained from the numerical simulation and experiments here, the non-constant stiffness distribution along the perimeter of this approach still requires further investigation. In addition, the

consideration of a non-prismatic inner shape of the insert is proposed for both aluminium and additive manufactured CFRP inserts to generalize this approach.

Acknowledgement

References

Adams, R.D. and Peppiatt, N.A. (1977), "Stress Analysis of Adhesive Bonded Tubular Lap Joints", *The Journal of Adhesion*, Vol. 9 No. 1, pp. 1–18. 10.1080/00218467708075095.

Albiez, M.F. (2016), "Zur statischen Tragfähigkeit geklebter Kreishohlprofilverbindungen im Stahlbau", Dissertation, Karlsruher Institut für Technologie, Karlsruhe, 2016. 10.5445/KSP/1000057648.

ANSYS, I. (2021), "Ansys Mechanical. Finite Element Analysis (FEA) Software for Structural Engineering", available at: https://www.ansys.com/products/structures/ansys-mechanical.

CG TEC GmbH (2021), "CFK - Profiles and connectors", available at: https://www.carbonscout-shop.de/Profiles-and-connectors.html.

Habenicht, G. (2009), *Kleben: Grundlagen, Technologien, Anwendungen*, 6th ed., Springer Berlin Heidelberg, Berlin, Heidelberg. 10.1007/978-3-540-85266-7.

Hart-Smith, L.J. (1973), *Adhesive-bonded double-lap joints*, Hampton, Virginia.

Jäger, M., Völkl, H. and Wartzack, S. (2020), "Konzept einer CAE-Methode zur systematischen Auslegung beanspruchungsgerechter; kurzfaserverstärkter AM-Fachwerksknoten für hochoptimierte Fachwerke", in *Proceedings of the 31st Symposium Design for X (DFX2020)*, *16-17 December* 2020, The Design Society, pp. 131–140. 10.35199/dfx2020.14.

Klein, D. (2017), Ein simulationsbasierter Ansatz für die beanspruchungsgerechte Auslegung endlosfaserverstärkter Faserverbundstrukturen, Konstruktionstechnik/Maschinenelemente, Vol. 439, 1. Auflage, VDI Verlag, Düsseldorf. 10.51202/9783186439017.

Lubkin, J.L. and Reissner, E. (1956), "Stress distributions and design data for adhesive lap joints between circular tubes", *Journal of Applied Mechanics*, No. 78, pp. 1213–1221.

Nemeş, O., Lachaud, F. and Mojtabi, A. (2006), "Contribution to the study of cylindrical adhesive joining", *International Journal of Adhesion and Adhesives*, Vol. 26 No. 6, pp. 474–480. 10.1016/j.ijadhadh.2005.07.009.

Pasternak, H., Hoch, H.-U. and Füg, D. (2010), *Stahltragwerke im Industriebau, EBL-Schweitzer*, Ernst, Berlin. 10.1002/9783433600535.

Pramanik, A., Basak, A.K., Dong, Y., Sarker, P.K., Uddin, M.S., Littlefair, G., Dixit, A.R. and Chattopadhyaya, S. (2017), "Joining of carbon fibre reinforced polymer (CFRP) composites and aluminium alloys – A review", *Composites Part A: Applied Science and Manufacturing*, Vol. 101, pp. 1–29. 10.1016/j.compositesa.2017.06.007.

Schürmann, H. (2007), *Konstruieren mit Faser-Kunststoff-Verbunden, VDI-Buch*, 2., bearbeitete und erweiterte Auflage, Springer-Verlag Berlin Heidelberg, Berlin, Heidelberg. 10.1007/978-3-540-72190-1.

Schütze, R. (1997), "Lightweight carbon fibre rods and truss structures", *Materials & Design*, Vol. 18 No. 4-6, pp. 231–238. 10.1016/S0261-3069(97)00056-3.

Siebert, M. (2006), Untersuchung der mechanischen Eigenschaften injektionsgefügter Rundsteckverbindungen, Zugl.: Kassel, Univ., Diss., 2006, Schriftenreihe des Instituts für Werkstofftechnik Kassel, Shaker, Aachen.

Volkersen, O. (1938), "Die Nietkraftverteilung in zugbeanspruchten Nietverbindungen mit konstanten Laschenquerschnitten", in *Luftfahrtforschung: Band 15*, Vol. 15, pp. 41–47.

Walbrun, S., Witzgall, C. and Wartzack, S. (2019), "A rapid CAE-based design method for modular hybrid truss structures", *Design Science*, Vol. 5. 10.1017/dsj.2019.26.